Z. angew. Math. Phys. 56 (2005) 497–515
0044-2275/05/030497-19
DOI 10.1007/s00033-004-2027-1

Zeitschrift für angewandte Mathematik und Physik ZAMP

Statistical ensemble error bounds for homogenized microheterogeneous solids

T. I. Zohdi

Abstract. Typically, in order to characterize the homogenized effective macroscopic response of new materials possessing random heterogeneous microstructure, a relation between averages $\langle \boldsymbol{\sigma} \rangle_\Omega = \mathbb{E}^* : \langle \boldsymbol{\epsilon} \rangle_\Omega$ is sought, where $\langle \cdot \rangle_\Omega \stackrel{\text{def}}{=} \frac{1}{|\Omega|} \int_\Omega \cdot \, d\Omega$, and where $\boldsymbol{\sigma}$ and $\boldsymbol{\epsilon}$ are the stress and strain tensor fields within a statistically representative volume element (SRVE) of volume $|\Omega|$. The quantity, $\mathbb{E}^*$, is known as the effective property, and is the elasticity tensor used in usual macroscale analyses. In order to generate homogenized responses computationally, a series of detailed boundary value representations resolving the heterogeneous microstructure, posed over the SRVE's domain, must be solved. This requires an enormous numerical effort that can overwhelm most computational facilities. A natural way of generating an approximation to the SRVE's response is by first computing the response of smaller (subrepresentative) samples, each with a different random realization of the microstructural type under investigation, and then to ensemble average the results afterwards. Compared to a direct simulation of an SRVE, testing many small samples is a computationally inexpensive process since the number of floating point operations is greatly reduced, as well as the fact that the samples' responses can be computed trivially in parallel. However, there is an inherent error in this process. Clearly the population's ensemble average is not the SRVE's response. However, as shown in this work, the moments on the distribution of the population can be used to generate rigorous upper and lower error bounds on the quality of the ensemble-generated response. Two-sided bounds are given on the SRVE response in terms of the ensemble average, its standard deviation and its skewness.

Keywords. Ensemble error bounds, homogenized properties, higher order moments.

1. Introduction

The success of many engineering designs stems from the use of microstructurally tailored materials. A relatively inexpensive way to obtain desired macroscopic material responses is to enhance the properties of a base matrix material by randomly dispersing foreign microscopic particles. Such materials offer a lower cost of manufacturing and greater formability compared to traditional continuous fiber-reinforced materials. The macroscopic response of such microscopically-modified base materials is the aggregate behavior of the assemblage of particles suspended in the binding matrix material. In the construction of such materials, the ba-

sic philosophy is to select material combinations in order to produce aggregate responses possessing desirable properties from each component. For example, in structural engineering applications, the classical choice is a particulate phase that serves as a stiffening agent for a base matrix material, although in many modern day designs the concerns are wide ranging, from increasing fracture toughness to tailoring thermal, acoustical and piezoelectrical properties. In order to accelerate laboratory development of new materials, it is now commonly accepted that numerical simulation is an important component in the analysis and design of micro-macro structural response relationships.[1]

1.1. Basic concepts in macro-micro modeling

We consider the case of linear elasticity. In this context, the mechanical properties of microheterogeneous materials are characterized by a spatially variable elasticity tensor $\mathbb{E}$. Typically, in order to characterize the (homogenized) effective macroscopic response of such materials, a relation between averages $\langle \boldsymbol{\sigma} \rangle_\Omega = \mathbb{E}^* : \langle \boldsymbol{\epsilon} \rangle_\Omega$ is sought, where $\langle \cdot \rangle_\Omega \stackrel{\text{def}}{=} \frac{1}{|\Omega|} \int_\Omega \cdot \, d\Omega$, and where $\boldsymbol{\sigma}$ and $\boldsymbol{\epsilon}$ are the stress and strain tensor fields within a statistically representative volume element (SRVE) of volume $|\Omega|$. The quantity, $\mathbb{E}^*$, is known as the effective property, and is the elasticity tensor used in usual macroscale analyses. Such regularization processes are referred to as "homogenization", "mean field theories", "theories of effective properties", etc. See Aboudi [1], Jikov et. al. [36], Mura [45], Nemat-Nasser and Hori [46] or Torquato [52]-[55] for reviews. In a similar manner, one can describe other effective quantities such as conductivity or diffusivity relating other volumetrically averaged field variables. However, for the sake of brevity, we restrict our analysis to linear elastostatics. It is clear that for the relation between averages to be statistically representative, it must be computed over a sample containing a significant amount of material. Within the last 100 years, due to the complexity of such problems, many approximate analytical methods for estimating the macroscopic responses of materials, based on a priori adhoc assumptions on the microstructural response, have been developed. Succinctly stated, such models require extensive experimental data to "tune" parameters that have little or no physical significance. Such inadequacies have led to computational approaches which require relatively simple descriptions on the microscale, leaving the majority of the effort to large-scale computing.

[1] There are a variety of terms which refer to intentionally doped microheterogeneous solids, for example, "composites", "new materials", "tailored solids" or "advanced solids". Since the terms are essentially synonymous, we use them interchangeably.

1.2. Mathematical setting

The computation of effective properties (the $\mathbb{E}^*$'s) requires a somewhat precise mathematical statement. Consider a sample of heterogeneous material occupying an open bounded domain in $\Omega \in \mathcal{R}^3$, under a given set of specified boundary loadings. Its boundary is denoted $\partial\Omega$. The body is in static equilibrium under the action of body forces, $\boldsymbol{f}$, and surface tractions, $\boldsymbol{t}$. The boundary $\overline{\partial\Omega} = \overline{\Gamma_u \cup \Gamma_t}$ consists of a part Γ_u and a part Γ_t on which displacements and tractions are respectively prescribed. Following standard notation, $H^1(\Omega)$ is denoted as the usual space of functions with generalized partial derivatives of degree ≤ 1 in $L^2(\Omega)$. The symbol $\boldsymbol{H}^1(\Omega) \stackrel{\text{def}}{=} [H^1(\Omega)]^3$ is defined as the space of vector-valued functions whose components have generalized partial derivatives ≤ 1 in $\boldsymbol{L}^2(\Omega) \stackrel{\text{def}}{=} [L^2(\Omega)]^3$. The symbol "$\boldsymbol{u}|_{\partial\Omega}$" is used for generalized boundary values, for example for specified boundary displacements. Throughout the analysis, the microstructure is assumed to be perfectly bonded. A general variational boundary value representation is: Find $\boldsymbol{u} \in \boldsymbol{H}^1(\Omega)$, $\boldsymbol{u}|_{\Gamma_u} = \boldsymbol{d}$, such that $\int_\Omega \nabla \boldsymbol{v} : \mathbb{E} : \nabla \boldsymbol{u}\, d\Omega = \int_\Omega \boldsymbol{f} \cdot \boldsymbol{v}\, d\Omega + \int_{\Gamma_t} \boldsymbol{t} \cdot \boldsymbol{v}\, dA$, $\forall \boldsymbol{v} \in \boldsymbol{H}^1(\Omega), \boldsymbol{v}|_{\Gamma_u} = \boldsymbol{0}$. The data are assumed to be such that $\boldsymbol{f} \in \boldsymbol{L}^2(\Omega)$ and $\boldsymbol{t} \in \boldsymbol{L}^2(\Gamma_t)$, however less smooth data can be considered without complications. It is convenient to consider the sample domain (Ω) as a cube, although, strictly speaking, this is not necessary. A commonly accepted macro/micro criterion used in effective property calculations is the well-known Hill condition (Hill [28]), $\langle \boldsymbol{\sigma} : \boldsymbol{\epsilon} \rangle_\Omega = \langle \boldsymbol{\sigma} \rangle_\Omega : \langle \boldsymbol{\epsilon} \rangle_\Omega$. Hill's condition dictates the size requirements on the sample to be statistically representative. The classical argument is as follows. For any perfectly bonded heterogeneous body, in the absence of body forces ($\boldsymbol{f} = \boldsymbol{0}$), two physically relevant loading states satisfy Hill's condition. They are (1) pure linear boundary displacements of the form $\boldsymbol{u}|_{\partial\Omega} = \mathcal{E} \cdot \boldsymbol{x}$, which implies $\langle \boldsymbol{\epsilon} \rangle_\Omega = \mathcal{E}$ and (2) pure boundary tractions in the form $\boldsymbol{t}|_{\partial\Omega} = \mathcal{L} \cdot \boldsymbol{n}$, which implies $\langle \boldsymbol{\sigma} \rangle_\Omega = \mathcal{L}$, where $\mathcal{E}$ and $\mathcal{L}$ are constant strain and stress tensors, respectively. Clearly, for Hill's condition to be satisfied within a macroscopic body under nonuniform external loading, the sample must be large enough to possess small boundary field fluctuations relative to its size. Therefore applying either of the two mentioned types of boundary conditions to a large sample is a way of reproducing approximately what may be occurring in a statistically representative mesoscopic subdomain of material within a macroscopic body.[2] Explicitly, to determine $\mathbb{E}^*$, one specifies six linearly independent loadings of the form, (1) $\boldsymbol{u}|_{\partial\Omega} = \mathcal{E}^{(I \to VI)} \cdot \boldsymbol{x}$ or (2) $\boldsymbol{t}|_{\partial\Omega} = \mathcal{L}^{(I \to VI)} \cdot \boldsymbol{n}$, where $\mathcal{E}^{(I \to VI)}$ and $\mathcal{L}^{(I \to VI)}$ are symmetric second order strain and stress tensors, with spatially constant components. Each independent loading state provides six equations, for a total of 36, which are used to determine the tensor relation between average stress and strain, $\mathbb{E}^*$. If the effective response is assumed isotropic, then only one test loading (instead of the usual six), possessing non-zero dilatational ($\frac{tr\boldsymbol{\sigma}}{3}$ and $\frac{tr\boldsymbol{\epsilon}}{3}$)

[2] If the sample were infinite in size in comparison to the length scales of the microstructure, and $\mathcal{L} = \mathbb{E}^* : \mathcal{E}$, then these test loading would be identical.

and deviatoric components ($\boldsymbol{\sigma}'$ and $\boldsymbol{\epsilon}'$), is necessary to determine the effective bulk and shear moduli, $3\kappa^* \stackrel{\text{def}}{=} \frac{\langle \frac{tr\boldsymbol{\sigma}}{3} \rangle_\Omega}{\langle \frac{tr\boldsymbol{\epsilon}}{3} \rangle_\Omega}$ and $2\mu^* \stackrel{\text{def}}{=} \sqrt{\frac{\langle \boldsymbol{\sigma}' \rangle_\Omega : \langle \boldsymbol{\sigma}' \rangle_\Omega}{\langle \boldsymbol{\epsilon}' \rangle_\Omega : \langle \boldsymbol{\epsilon}' \rangle_\Omega}}$.

1.3. Size effects in computational materials testing

In order to perform meaningful characterizations of new materials with inherently heterogeneous microstructure, one needs reliable effective responses. It is clear that for the relation between averages to be useful, i.e. statistically representative, the sample must be so large that, for further enlargements, $\boldsymbol{I\!E}^*$ changes minimally. Unfortunately, detailed boundary value representations resolving the heterogeneous microstructure require an enormous numerical effort that can overwhelm even the most modern computational facilities. In short, solutions to partial differential equations posed over statistically representative samples of irregular microheterogeneous material are still open problems, *even in the case of linearized elasticity.* Therefore, due to the inability to directly simulate a statistically representative volume element, one must settle for computing responses of sub-statistically representative, finite sized, samples. Computationally, it is clear that testing many small samples is less expensive since the number of floating point operations is less, as well as the fact that the samples' responses can be computed in parallel. For example, if one considers a large cubical domain, whose response is simulated using n numerical unknowns, for example employing a finite element discretization, approximately $\mathcal{O}(n^\gamma)$ floating point operations are needed to solve the system. The value of γ, typically $2 \leq \gamma \leq 3$, depends on the type of algebraic system solver used. If the cube was divided into N equal subdomains (subcubes), the number of floating point operations needed would be approximately on the order of $\left(\frac{n}{N}\right)^\gamma N$, and thus $DIRECT\ COSTS/DECOMPOSED\ COSTS \approx N^{\gamma-1}$. For example, if one had 1000 subdomains, the "broken" solution costs between 1000 and 1000000 times less to compute than the globally exact solution. The advantages are not limited to the possible reduction of operation counts. If one includes the inherent trivial paralellization, then the ratio of costs becomes $PN^{\gamma-1}$, where P denotes the number of processors. However, a primary problem associated with computing macroscopic effective mechanical responses of relatively small finite sized samples of materials, possessing heterogeneous irregular microstructure is that equal sized samples exhibit mutual fluctuations from one another, i.e. no single effective response ($\boldsymbol{I\!E}^*$) will be obtained, but rather a distribution of responses, $\boldsymbol{I\!E}^* \pm \Delta\boldsymbol{I\!E}^*$, even for relatively large groups of particles.[3]

Following Zohdi and Wriggers [62], we considered a set of tests where the number of (spherical) randomly dispersed particles contained in a sample were increased holding the volume fraction constant. During the tests, we repeatedly

[3]It is obvious that if the samples were infinite in size relative to the particles, there would be no fluctuations in the responses, but clearly this is impossible to test from either a computational or experimental point of view.

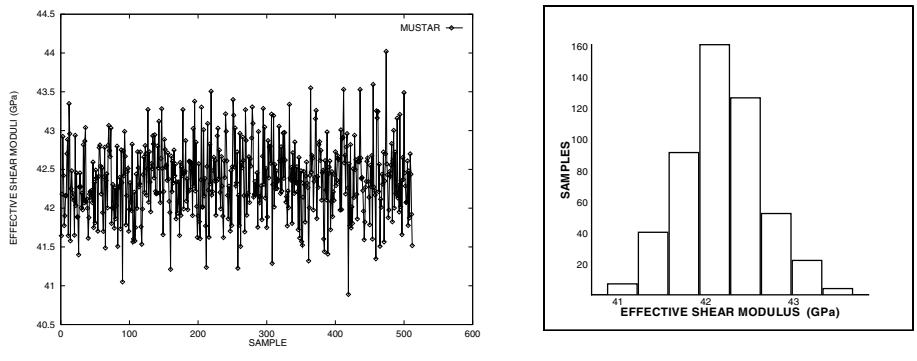

Figure 1. RIGHT: The shear responses, μ^*, of 512 equally sized samples each with 20 randomly distributed Boron spheres embedded in an Aluminum matrix. Each point represents the results of one test. LEFT: The corresponding histogram for the variations in the effective shear responses, μ^*. The data are from Zohdi et al. [64].

refined the mesh to obtain invariant macroscopic responses. For illustration purposes, we used an Aluminum (matrix)/Boron (particle) combination, which offers a high strength lightweight alternative to steels. The Boron ($\kappa = 230\,GPa$, $\mu = 172\,GPa$) is used as a stiffener for the Aluminum matrix ($\kappa = 77.9\,GPa$, $\mu = 24.9\,GPa$). We used a moderate particulate volume fraction of approximately 22 %. For a variety of numerical tests, discussed momentarily, the typical mesh density to deliver mesh insensitive volumetrically ensemble averaged responses was $9 \times 9 \times 9$ trilinear finite element hexahedra (approximately 2200-3000 degrees of freedom (DOF)) *per particle*. The following particle per sample sequence was used to study the dependence of the effective responses on the sample size: 2 (5184 DOF), 4 (10125 DOF), 8 (20577 DOF), 16 (41720 DOF), 32 (81000 DOF) and 64 (151959 DOF) particles. In order to get more reliable response data for each particle number set, the tests were performed 100 times for each sample size (each time with a different random particulate distribution) and the responses averaged. A meaningful parameter to track was the ratio of the diameter of the individual particles (d) to the length of the sample (L). Throughout the tests, we considered a single combined boundary loading satisfying Hill's condition, $\boldsymbol{u}|_{\partial\Omega} = \boldsymbol{\mathcal{E}} \cdot \boldsymbol{x}$, $\mathcal{E}_{ij} = 0.001, i, j = 1, 2, 3$. We tracked the effective bulk and shear moduli, κ^* and μ^*, respectively. Since the effective bulk and shear responses behave in a quantitatively similar manner, for brevity, we show only the effective shear responses. Motivated by the fact that for three successive enlargements of the number of particles, i.e. 16, 32 and 64 particle samples (the responses differed from one another, on average, by less than 1 %), we selected the 20-particle microstructures for further tests.[4] Following Zohdi et al. [64], we then simulated 512 different samples,

[4] A "2/5" Gauss rule was used, whereby elements with discontinuities had increased Gauss rules ($5 \times 5 \times 5$) to increase the resolution of the internal geometry, while elements with no discontinuities had the nominal $2 \times 2 \times 2$ rule. For more details on such simulation techniques see Zohdi and Wriggers [62].

each time with a different random distribution of 20 nonintersecting particles occupying 22 % of the volume. Consistent with the previous test's mesh densities, we found that beyond approximately 2344 DOF per particle ($24 \times 24 \times 24$ mesh or $9 \times 9 \times 9$ trilinear hexahedra or 46875 DOF per test sample), the numerical simulations were insensitive to further mesh refinements. As one can see in Figure 1, the fluctuation in the response is roughly seven percent. Detailed studies and reviews addressing size effects in effective responses of heterogeneous media can be found in Huet [30]–[32], Hazanov and Huet [26], Hazanov and Amieur [27] and Huet [34], [35]. It is clear that the effects of fluctuations due to sample size can undermine the ability to accurately compare responses for material design changes, for example changes in the particulate material's volume fraction, phase contrasts (stiffness mismatches) or topologies. We refer the interested reader to Zohdi [65] for design case studies. A natural way of generating an approximation to the SRVE's response is by ensemble averaging the responses of smaller samples, such as the ones just presented. However, the population's ensemble average is not the SRVE's response. However, as we proceed to prove, the moments of the distribution of the population can be used to generate rigorous upper and lower error bounds of the quality of the ensemble-generated response. Two-sided bounds are given on the ensemble average, its standard deviation and its skewness, i.e. the symmetry of the distribution.

Remarks: The upcoming results can be used in conjunction with a variety of methods to perform large-scale micro-macro simulations. Noteworthy are the multiscale methods: Fish and Wagiman [6], Fish et. al [7], Fish and Belsky [8], Fish and Belsky [9], Fish and Belsky [10], Fish et. al [11], Fish et. al [12], Fish and Shek [13], Fish and Ghouli [14], Fish and Yu [15], Fish and Chen [16], Chen and Fish [5] and Wentorf et. al [58], Voronoi cell methods: Ghosh and Mukhopadhyay [18], Ghosh and Moorthy [19], Ghosh et. al [20], Ghosh and Moorthy [21], Ghosh et. al [22], Ghosh et. al [23], Lee et. al [38], Li et. al [40], Moorthy and Ghosh [43] and Raghavan et. al [50], transformation methods: Moulinec et. al [44] and Michel et al. [41], partitioning methods: Huet [30], [31], [32], Hazanov and Huet [26], Hazanov and Amieur [27] and Huet [34], [35] and the adaptive hierarchical modeling methods: Zohdi et. al [59], Oden and Zohdi [47], Moes et. al [42], Oden and Vemaganti [48], Oden et. al [49] and Vemaganti and Oden [56] and finally multipole methods adapted to such problems by Fu et. al [17]. Particularly, attractive are iterative domain decomposition type strategies, whereby a global domain is divided into nonoverlapping subdomains. On the interior subdomain partitions an approximate globally kinematically admissible displacement is projected. This allows the subdomains to be mutually decoupled, and therefore separately solvable. The subdomain boundary value problems are solved with the exact microstructural representation contained within their respective boundaries, but with approximate displacement boundary data. The resulting microstructural solution is the assembly of the subdomain solutions, each restricted to its corresponding subdomain. As in the ensemble testing, the approximate solution is far

more inexpensive to compute than the direct problem. Numerical and theoretical studies of such approaches have been studied in Huet [30], Hazanov and Huet [26], Zohdi et. al [59], Oden and Zohdi [47], Zohdi and Wriggers [60],[62],[63], Zohdi [61] and Zohdi et. al [64]. Clearly, when decomposing the structure by a projection of a kinematically admissible function onto the partitioning interfaces, regardless of the constitutive law, the error is due to the jumps in tractions at the interfaces (statical inadmissibility). If the interfaces would be in equilibrium, then there would be no traction jumps. Therefore, if the resulting approximate solution is deemed not accurate enough, via a posteriori error estimation techniques, the decoupling function on the boundaries of the subdomain is updated using information from the previously computed solution, and the subdomains are resolved. Methods for updating subdomain boundaries can be found in Zohdi et. al [64]. They bear a strong relation to alternating Schwarz domain decomposition methods (see Le Tallec [39] for reviews) and methods of equilibration, i.e. balancing traction jumps at subdomain interfaces (see Ainsworth and Oden [2]).

2. Statistical shifting theorems

Consider any tested quantity, Q, with a distribution of values (Q_i, $i = 1, 2, ...N =$ samples) about an arbitrary reference point, denoted $Q^\star$, as follows:

$$\boldsymbol{M}_r^{Q_i - Q^\star} \stackrel{\text{def}}{=} \frac{\sum_{i=1}^{N} (Q_i - Q^\star)^r}{N} \stackrel{\text{def}}{=} \overline{(Q_i - Q^\star)^r}, \tag{1}$$

where $\frac{\sum_{i=1}^{N}(\cdot)}{N} \stackrel{\text{def}}{=} \overline{(\cdot)}$ and $A \stackrel{\text{def}}{=} \overline{Q_i}$. The various moments characterize the distribution, for example: (1) $\boldsymbol{M}_1^{Q_i - A}$ measures the first deviation from the average, which equals zero, (2) $\boldsymbol{M}_1^{Q_i - 0} \stackrel{\text{def}}{=} \frac{\sum_{i=1}^{N}(Q_i - 0)}{N} \stackrel{\text{def}}{=} \overline{(Q_i - 0)} = A$, (3) $\boldsymbol{M}_2^{Q_i - A}$ is the standard deviation and (4) $\boldsymbol{M}_3^{Q_i - A}$ is the skewness. The skewness measures the bias, or asymmetry of the distribution of data. The moments of the data can be expressed about the average and related to any other reference point, denoted here as Q^*, using parallel axis type theorems. Using the notation in Equation 1, let us define $q_i = Q_i - A \Rightarrow \overline{Q_i = A + q_i} \Rightarrow \overline{Q_i} = A + \overline{q_i} \Rightarrow Q_i - \overline{Q_i} = q_i - \overline{q_i}$. There are useful properties associated with these relations, in particular a shifting property for the standard deviation

$$\begin{aligned} \boldsymbol{M}_2^{Q_i - A} \stackrel{\text{def}}{=} \overline{(Q_i - A)^2} &= \overline{(q_i - \overline{q_i})^2} = \overline{q_i^2 - 2\overline{q_i} q_i + \overline{q_i}^2}, \\ &= \overline{q_i^2} - 2\overline{q_i}^2 + \overline{q_i}^2, \\ &= \overline{q_i^2} - \overline{q_i}^2, \\ &= \boldsymbol{M}_2^{Q_i - Q^*} - (\boldsymbol{M}_1^{Q_i - Q^*})^2, \end{aligned} \tag{2}$$

as well as for the skewness

$$\begin{aligned}\boldsymbol{M}_3^{Q_i-A} \stackrel{\text{def}}{=} \overline{(Q_i-A)^3} &= \overline{(q_i-\overline{q_i})^3} = \overline{q_i^3 - 3q_i^2\overline{q_i} + 3\overline{q_i}^2 q_i - \overline{q_i}^3},\\ &= \overline{q_i^3} - 3\overline{q_i^2}\overline{q_i} + 2\overline{q_i}^3,\\ &= \boldsymbol{M}_3^{Q_i-Q^*} - 3(\boldsymbol{M}_1^{Q_i-Q^*})(\boldsymbol{M}_2^{Q_i-Q^*}) + 2(\boldsymbol{M}_1^{Q_i-Q^*})^3.\end{aligned} \tag{3}$$

From Equation 2 we may write

$$\begin{aligned}3(\boldsymbol{M}_1^{Q_i-Q^*})(\boldsymbol{M}_2^{Q_i-Q^*}) - 2(\boldsymbol{M}_1^{Q_i-Q^*})^3 &= \boldsymbol{M}_1^{Q_i-Q^*}\left(3(\boldsymbol{M}_2^{Q_i-Q^*}) - 2(\boldsymbol{M}_1^{Q_i-Q^*})^2\right),\\ &= \boldsymbol{M}_1^{Q_i-Q^*}\left(\boldsymbol{M}_2^{Q_i-Q^*} + 2(\boldsymbol{M}_2^{Q_i-Q^*}) - 2(\boldsymbol{M}_1^{Q_i-Q^*})^2\right),\\ &= \boldsymbol{M}_1^{Q_i-Q^*}\left(\boldsymbol{M}_2^{Q_i-Q^*} + 2\boldsymbol{M}_2^{Q_i-A}\right),\end{aligned} \tag{4}$$

and therefore,

$$\boldsymbol{M}_3^{Q_i-A} + \boldsymbol{M}_1^{Q_i-Q^*}\left(\boldsymbol{M}_2^{Q_i-Q^*} + 2\boldsymbol{M}_2^{Q_i-A}\right) = \boldsymbol{M}_3^{Q_i-Q^*}. \tag{5}$$

We now proceed to bound the average, standard deviation and skewness associated with the ensemble averaging of a population of samples.

3. Domain decomposition and ensemble averaging

3.1. Primal partitioning

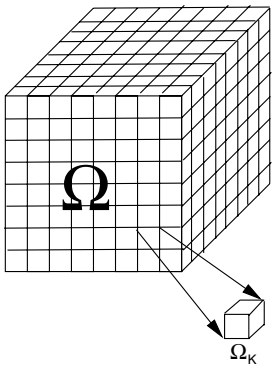

Figure 2. A regular partitioning of a large sample of material.

Consider a (statistically representative) sample of material with the following general boundary value representation

$$\text{Find } \boldsymbol{u} \in \boldsymbol{H}^1(\Omega), \boldsymbol{u}|_{\Gamma_u} = \boldsymbol{d}, \text{ such that}$$

$$\int_\Omega \nabla \boldsymbol{v} : \underbrace{\boldsymbol{I\!E} : \nabla \boldsymbol{u}}_{\boldsymbol{\sigma}} \, d\Omega = \int_\Omega \boldsymbol{f} \cdot \boldsymbol{v} \, d\Omega + \int_{\Gamma_t} \boldsymbol{t} \cdot \boldsymbol{v} \, dA, \quad \forall \boldsymbol{v} \in \boldsymbol{H}^1(\Omega), \boldsymbol{v}|_{\Gamma_u} = \boldsymbol{0}. \tag{6}$$

Now partition the domain into S subdomains, $\Omega = \cup_{K=1}^{S} \Omega_K$. The pieces do not have to be the same size or shape, although for illustration purposes it is convenient to use a uniform (regular) partitioning (Figure 2). Consider a kinematically admissible function, $\boldsymbol{U} \in \boldsymbol{H}^1(\Omega)$ and $\boldsymbol{U}|_{\Gamma_u} = \boldsymbol{d}$, which is projected onto the *internal boundaries* ($\partial\Omega_K$) of the subdomains. Any subdomain boundaries coinciding with the exterior surface retain their original boundary conditions (Figure 2). Accordingly, we have the following virtual work formulation, for each subdomain, $1 \leq K \leq S$:

$$\text{Find } \tilde{\boldsymbol{u}}_K \in \boldsymbol{H}^1(\Omega_K), \tilde{\boldsymbol{u}}_K|_{\partial\Omega_K \cap (\Omega \cup \Gamma_u)} = \boldsymbol{U} \in \boldsymbol{H}^1(\Omega), \text{ such that}$$

$$\int_{\Omega_K} \nabla \boldsymbol{v}_K : \underbrace{\boldsymbol{I\!E} : \nabla \tilde{\boldsymbol{u}}_K}_{\tilde{\boldsymbol{\sigma}}_K} \, d\Omega = \int_{\Omega_K} \boldsymbol{f} \cdot \boldsymbol{v}_K \, d\Omega + \int_{\partial\Omega_K \cap \Gamma_t} \boldsymbol{t} \cdot \boldsymbol{v}_K \, dA \tag{7}$$

$$\forall \boldsymbol{v}_K \in \boldsymbol{H}^1(\Omega_K), \boldsymbol{v}_K|_{\partial\Omega_K \cap (\Omega \cup \Gamma_u)} = \boldsymbol{0}.$$

The individual subdomain solutions, $\tilde{\boldsymbol{u}}_K$, are zero outside of the corresponding subdomain $\overline{\Omega}_K$. In this case the approximate solution is constructed by a direct assembly process, $\tilde{\boldsymbol{u}} \overset{\text{def}}{=} \boldsymbol{U} + (\tilde{\boldsymbol{u}}_1 - \boldsymbol{U})|_{\Omega_1} + (\tilde{\boldsymbol{u}}_2 - \boldsymbol{U})|_{\Omega_2} + ... + (\tilde{\boldsymbol{u}}_S - \boldsymbol{U})|_{\Omega_S}$. The approximate displacement field is in $\boldsymbol{H}^1(\Omega)$, however, the approximate traction field may possibly be discontinuous. Logical choices of $\boldsymbol{U}$, i.e. $\boldsymbol{U} = \mathcal{E} \cdot \boldsymbol{x}$, will be given momentarily. It should be clear that if $\boldsymbol{U} = \boldsymbol{u}$ on the internal partition boundaries, then the approximate solution is exact. Since we employ energy type variational principles to generate approximate solutions, we use an induced energy norm to measure the solution differences $0 \leq ||\boldsymbol{u} - \tilde{\boldsymbol{u}}||^2_{E(\Omega)} \overset{\text{def}}{=} \int_\Omega \nabla(\boldsymbol{u} - \tilde{\boldsymbol{u}}) : \boldsymbol{I\!E} : \nabla(\boldsymbol{u} - \tilde{\boldsymbol{u}}) \, d\Omega$. It is convenient to cast the error in terms of the potential energy, $\mathcal{J}(\boldsymbol{w}) \overset{\text{def}}{=} \frac{1}{2} \int_\Omega \nabla \boldsymbol{w} : \boldsymbol{I\!E} : \nabla \boldsymbol{w} \, d\Omega - \int_\Omega \boldsymbol{f} \cdot \boldsymbol{w} \, d\Omega - \int_{\Gamma_t} \boldsymbol{t} \cdot \boldsymbol{w} \, dA$, where $\boldsymbol{w}$ is any kinematically admissible function. This leads to $||\boldsymbol{u} - \boldsymbol{w}||^2_{E(\Omega)} = 2(\mathcal{J}(\boldsymbol{w}) - \mathcal{J}(\boldsymbol{u}))$ or $\mathcal{J}(\boldsymbol{u}) \leq \mathcal{J}(\boldsymbol{w})$, which is a form of the Principle of Minimum Potential Energy. In other words, the true solution possesses a minimum potential. By direct substitution we have $||\boldsymbol{u} - \tilde{\boldsymbol{u}}||^2_{E(\Omega)} = 2(\mathcal{J}(\tilde{\boldsymbol{u}}) - \mathcal{J}(\boldsymbol{u}))$. In the special case that $\boldsymbol{u}|_{\partial\Omega} = \mathcal{E} \cdot \boldsymbol{x}$, which is equivalent to testing each subsample with $\boldsymbol{u}|_{\partial\Omega_K} = \mathcal{E} \cdot \boldsymbol{x}$ and $\boldsymbol{f} = \boldsymbol{0}$, then $||\boldsymbol{u} - \tilde{\boldsymbol{u}}||^2_{E(\Omega)} = \mathcal{E} : (\tilde{\boldsymbol{I\!E}}^* - \boldsymbol{I\!E}^*) : \mathcal{E}|\Omega|$, where $\langle \tilde{\boldsymbol{\sigma}} \rangle_{\Omega_K} \overset{\text{def}}{=} \tilde{\boldsymbol{I\!E}}^*_K : \langle \tilde{\boldsymbol{\epsilon}} \rangle_{\Omega_K}$

and $\tilde{\mathbb{E}}^* \stackrel{\text{def}}{=} \sum_{K=1}^{S} \tilde{\mathbb{E}}^*_K \frac{|\Omega_K|}{|\Omega|}$.

3.2. Complementary partitioning

We can repeat the partitioning process for an applied internal traction set of tests. The equivalent complementary form for the exact (undecomposed) problem is

$$\begin{aligned} &\text{Find } \boldsymbol{\sigma}, \nabla \cdot \boldsymbol{\sigma} + \boldsymbol{f} = \boldsymbol{0}, \boldsymbol{\sigma} \cdot \boldsymbol{n}|_{\Gamma_t} = \boldsymbol{t} \ \text{ such that} \\ &\int_{\Omega} \boldsymbol{\tau} : \mathbb{E}^{-1} : \boldsymbol{\sigma} \, d\Omega = \int_{\Gamma_u} \boldsymbol{\tau} \cdot \boldsymbol{n} \cdot \boldsymbol{d} \, dA, \ \ \forall \boldsymbol{\tau}, \nabla \cdot \boldsymbol{\tau} = \boldsymbol{0}, \boldsymbol{\tau} \cdot \boldsymbol{n}|_{\Gamma_t} = \boldsymbol{0}. \end{aligned} \tag{8}$$

For the complementary problem, similar restrictions are placed on the solution and test fields to force the integrals to make sense. In other words, we assume that solutions produce finite global energy. When employing the applied internal traction approach, in order to construct approximate solutions, a statically admissible function, $\boldsymbol{\Sigma}$, with the property that $\boldsymbol{\Sigma} \cdot \boldsymbol{n}|_{\Gamma_t} = \boldsymbol{t}$, is projected onto the *internal boundaries* of the subdomain partitions. As in the applied displacement case, any subdomain boundaries coinciding with the exterior surface retain their original boundary conditions. Accordingly, we have the following complementary virtual work formulation, for each subdomain, $1 \leq K \leq S$:

$$\begin{aligned} &\text{Find } \hat{\boldsymbol{\sigma}}_K, \nabla \cdot \hat{\boldsymbol{\sigma}}_K + \boldsymbol{f} = \boldsymbol{0}, \hat{\boldsymbol{\sigma}}_K \cdot \boldsymbol{n}|_{\partial\Omega_K \cap (\Omega \cup \Gamma_t)} = \boldsymbol{\Sigma} \cdot \boldsymbol{n}|_{\partial\Omega_K \cap (\Omega \cup \Gamma_t)} \ \text{ such that} \\ &\int_{\Omega_K} \boldsymbol{\tau}_K : \mathbb{E}^{-1} : \hat{\boldsymbol{\sigma}}_K \, d\Omega = \int_{\Gamma_u} \boldsymbol{\tau}_K \cdot \boldsymbol{n} \cdot \boldsymbol{d} \, dA \\ &\forall \boldsymbol{\tau}_K, \nabla \cdot \boldsymbol{\tau}_K = \boldsymbol{0}, \boldsymbol{\tau}_K \cdot \boldsymbol{n}|_{\partial\Omega_K \cap (\Omega \cup \Gamma_t)} = \boldsymbol{0}. \end{aligned} \tag{9}$$

The individual subdomain solutions, $\hat{\boldsymbol{\sigma}}_K$, are zero outside of the corresponding subdomain $\overline{\Omega}_K$. In this case the approximate solution is constructed by a direct assembly process $\hat{\boldsymbol{\sigma}} \stackrel{\text{def}}{=} \boldsymbol{\Sigma} + (\hat{\boldsymbol{\sigma}}_1 - \boldsymbol{\Sigma})|_{\Omega_1} + (\hat{\boldsymbol{\sigma}}_2 - \boldsymbol{\Sigma})|_{\Omega_2} + ... + (\hat{\boldsymbol{\sigma}}_S - \boldsymbol{\Sigma})|_{\Omega_S}$. The stress field is statically admissible, however, the approximate displacement field is possibly discontinuous. Logical choices of $\boldsymbol{\Sigma}$, $\boldsymbol{\Sigma} = \mathcal{L} = constant$, will be given momentarily. It should be clear that if $\boldsymbol{\Sigma} = \boldsymbol{\sigma}$ on the internal partition boundaries, then the approximate solution is exact. We define the complementary norm $0 \leq ||\boldsymbol{\sigma} - \hat{\boldsymbol{\sigma}}||^2_{E^{-1}(\Omega)} \stackrel{\text{def}}{=} \int_{\Omega} (\boldsymbol{\sigma} - \hat{\boldsymbol{\sigma}}) : \mathbb{E}^{-1} : (\boldsymbol{\sigma} - \hat{\boldsymbol{\sigma}}) \, d\Omega$. As in the primal case, it is convenient to cast the error in terms of the potential complementary energy for the case of linear elasticity, where $\mathcal{K}(\boldsymbol{\gamma}) \stackrel{\text{def}}{=} \frac{1}{2} \int_{\Omega} \boldsymbol{\gamma} : \mathbb{E}^{-1} : \boldsymbol{\gamma} \, d\Omega - \int_{\Gamma_u} \boldsymbol{\gamma} \cdot \boldsymbol{n} \cdot \boldsymbol{u} \, dA$, where $\boldsymbol{\gamma}$ is any statically admissible function. The well known relationship, for a statically admissible function $\boldsymbol{\gamma}$, is $||\boldsymbol{\sigma} - \boldsymbol{\gamma}||^2_{E^{-1}(\Omega)} = 2(\mathcal{K}(\boldsymbol{\sigma}) - \mathcal{K}(\boldsymbol{\sigma}))$ or $\mathcal{K}(\boldsymbol{\sigma}) \leq \mathcal{K}(\boldsymbol{\gamma})$. This

is a form of the Principle of Minimum Complementary Potential Energy. In other words, the true solution possesses a minimum complementary potential. Choosing $\boldsymbol{\gamma} = \hat{\boldsymbol{\sigma}}$, we have $||\boldsymbol{\sigma} - \hat{\boldsymbol{\sigma}}||^2_{E(\Omega)} = 2(\mathcal{K}(\hat{\boldsymbol{\sigma}}) - \mathcal{K}(\boldsymbol{\sigma}))$. In the special case that $\boldsymbol{t}|_{\partial\Omega} = \mathcal{L} \cdot \boldsymbol{n}$, which is equivalent to testing each subsample with $\boldsymbol{t}|_{\partial\Omega_K} = \mathcal{L} \cdot \boldsymbol{n}$, $||\boldsymbol{\sigma} - \hat{\boldsymbol{\sigma}}||^2_{E^{-1}(\Omega)} = \mathcal{L} : (\hat{\boldsymbol{I\!E}}^{-1*} - \boldsymbol{I\!E}^{-1*}) : \mathcal{L}|\Omega|$, where $\langle\hat{\boldsymbol{\epsilon}}\rangle_{\Omega_K} \stackrel{\text{def}}{=} \hat{\boldsymbol{I\!E}}^{-1*}_K : \langle\hat{\boldsymbol{\sigma}}\rangle_{\Omega_K}$ and $\hat{\boldsymbol{I\!E}}^{-1*} \stackrel{\text{def}}{=} \sum_{K=1}^{S} \hat{\boldsymbol{I\!E}}^{-1*}_K \frac{|\Omega_K|}{|\Omega|}$.

3.3. Homogenized material orderings

If the sample is statistically representative, we have $\boldsymbol{I\!E}^{-1*} = \boldsymbol{I\!E}^{*-1}$, then the previous results imply, under the assumption that the uniform loadings are arbitrary, the following two sided ordering of approximate effective material responses,

$$\langle \boldsymbol{I\!E}^{-1} \rangle^{-1}_{\Omega} \leq \hat{\boldsymbol{I\!E}}^{*} \leq \boldsymbol{I\!E}^{*} \leq \tilde{\boldsymbol{I\!E}}^{*} \leq \langle \boldsymbol{I\!E} \rangle_{\Omega}, \tag{10}$$

where the tensor inequality notation means, for example, that $\mathcal{E} : \tilde{\boldsymbol{I\!E}}^{*} - \boldsymbol{I\!E}^{*} : \mathcal{E} \geq 0$ for all admissible $\mathcal{E}$, where the equality holds only if $\mathcal{E} = \boldsymbol{0}$. Since $\mathcal{J}(\tilde{\boldsymbol{u}}) \leq \mathcal{J}(\boldsymbol{U})$, we also have $\tilde{\boldsymbol{I\!E}}^{*} \leq \langle \boldsymbol{I\!E} \rangle_{\Omega}$. Alternatively, since $\mathcal{K}(\hat{\boldsymbol{\sigma}}) \leq \mathcal{K}(\mathcal{L})$, then $\hat{\boldsymbol{I\!E}}^{-1*} \leq \langle \boldsymbol{I\!E}^{-1} \rangle_{\Omega}$. For isotropic responses, we have

$$\begin{aligned} \langle \kappa^{-1} \rangle^{-1}_{\Omega} \leq \hat{\kappa}^{*} \leq \kappa^{*} \leq \tilde{\kappa}^{*} \leq \langle \kappa \rangle_{\Omega} \\ \langle \mu^{-1} \rangle^{-1}_{\Omega} \leq \hat{\mu}^{*} \leq \mu^{*} \leq \tilde{\mu}^{*} \leq \langle \mu \rangle_{\Omega}. \end{aligned} \tag{11}$$

To the knowledge of the author, the result in Equation 10 was first derived in Huet [32] by alternative means.

Remark: Voigt [57] (1889) is usually credited with the first analysis of the effective *mechanical* properties of the microheterogeneous solids, with a complementary contribution given later by Reuss [51] (1929). Voigt assumed that the strain field within an aggregate sample of heterogeneous material was uniform, leading to $\langle \boldsymbol{I\!E} \rangle_{\Omega}$ as an expression of the effective property, while the dual assumption was made by Reuss, who approximated the stress fields within the material as uniform. If the Reuss field is assumed within the SRVE, then an expression for the effective property is $\langle \boldsymbol{I\!E}^{-1} \rangle^{-1}_{\Omega}$. A fundamental result (Hill [28], 1952) is $\langle \boldsymbol{I\!E}^{-1} \rangle^{-1}_{\Omega} \leq \boldsymbol{I\!E}^{*} \leq \langle \boldsymbol{I\!E} \rangle_{\Omega}$. These inequalities mean that the eigenvalues of the tensors $\boldsymbol{I\!E}^{*} - \langle \boldsymbol{I\!E}^{-1} \rangle^{-1}_{\Omega}$ and $\langle \boldsymbol{I\!E} \rangle_{\Omega} - \boldsymbol{I\!E}^{*}$ are non-negative. Therefore, one can interpret the Voigt ([57] (1889)) and Reuss ([51] (1929)) fields as providing two microfield extremes, since the Voigt stress field is one where the tractions at the phase boundaries cannot be in equilibrium, i.e. statically inadmissible, while the implied Reuss strains are such that the heterogeneities and the matrix could not be perfectly bonded, i.e. kinematically inadmissible. Typically, the bounds are quite wide and provide only

rough qualitative information.

3.4. Embedded orthogonal monotonicities

Since $\tilde{\boldsymbol{u}}$ is kinematically admissible, we have $||\boldsymbol{u}-\tilde{\boldsymbol{u}}||^2_{E(\Omega)} = 2(\mathcal{J}(\tilde{\boldsymbol{u}}) - \mathcal{J}(\boldsymbol{u}))$. If we repartition the existing subdomains into more subdomains (Figure 3), and use $\boldsymbol{U}$ for the local boundary conditions on the finer partition, upon solving the local boundary value problems and assembling the local solutions together (just as before for $\tilde{\boldsymbol{u}}$), we have, denoting the solution by $\tilde{\tilde{\boldsymbol{u}}}$, $||\tilde{\boldsymbol{u}}-\tilde{\tilde{\boldsymbol{u}}}||^2_{E(\Omega)} = 2(\mathcal{J}(\tilde{\tilde{\boldsymbol{u}}})-\mathcal{J}(\tilde{\boldsymbol{u}}))$. Adding the two previous relations together yields an orthogonal decomposition

$$||\boldsymbol{u}-\tilde{\tilde{\boldsymbol{u}}}||^2_{E(\Omega)} = ||\tilde{\boldsymbol{u}}-\tilde{\tilde{\boldsymbol{u}}}||^2_{E(\Omega)} + ||\boldsymbol{u}-\tilde{\boldsymbol{u}}||^2_{E(\Omega)}. \tag{12}$$

This implies that the error monotonically grows for successively finer embedded partitions. Intuitively one expects this type of growth in the error, since one is projecting more inaccurate data onto the interfaces. *Simply stated, more embedded subdomains, more error. Furthermore, the relationship is monotone.* As in the displacement controlled tests, for traction controlled tests we have

$$||\boldsymbol{\sigma}-\hat{\tilde{\boldsymbol{\sigma}}}||^2_{E^{-1}(\Omega)} = ||\hat{\boldsymbol{\sigma}}-\hat{\tilde{\boldsymbol{\sigma}}}||^2_{E^{-1}(\Omega)} + ||\boldsymbol{\sigma}-\hat{\boldsymbol{\sigma}}||^2_{E^{-1}(\Omega)}. \tag{13}$$

In terms of effective properties, Equation 12 implies $\mathcal{E} : (\tilde{\boldsymbol{I\!E}}^* - \boldsymbol{I\!E}^*) : \mathcal{E} = \mathcal{E} : (\tilde{\tilde{\boldsymbol{I\!E}}}^* - \tilde{\boldsymbol{I\!E}}^*) : \mathcal{E} + \mathcal{E} : (\tilde{\boldsymbol{I\!E}}^* - \boldsymbol{I\!E}^*) : \mathcal{E}$, while Equation 13 implies $\mathcal{L} : (\hat{\tilde{\boldsymbol{I\!E}}}^{-1*} - \tilde{\boldsymbol{I\!E}}^{-1*}) : \mathcal{L} = \mathcal{L} : (\hat{\tilde{\boldsymbol{I\!E}}}^{-1*} - \hat{\boldsymbol{I\!E}}^{-1*}) : \mathcal{L} + \mathcal{L} : (\hat{\boldsymbol{I\!E}}^{-1*} - \boldsymbol{I\!E}^{-1*}) : \mathcal{L}$. To streamline the notation we employ the notation $\overset{\bar{\mathrm{Z}}}{\boldsymbol{I\!E}}{}^*$ to denote Z embedded partitions, etc. The higher the number the more embedded partitions exist (Figure 3). Therefore, for $1 \leq M \leq Z$ and $1 \leq P \leq L$, we have

$$\begin{aligned}\langle \boldsymbol{I\!E}^{-1}\rangle^{-1}_{\Omega} \leq ... \overset{\hat{\mathrm{L}}}{\boldsymbol{I\!E}}{}^* \leq \overset{\hat{\mathrm{P}}}{\boldsymbol{I\!E}}{}^* ... \\ \leq \hat{\boldsymbol{I\!E}}^* \leq \boldsymbol{I\!E}^* \leq \tilde{\boldsymbol{I\!E}}^* \leq ... \overset{\check{\mathrm{M}}}{\boldsymbol{I\!E}}{}^* \leq \overset{\bar{\mathrm{Z}}}{\boldsymbol{I\!E}}{}^* ... \leq \langle \boldsymbol{I\!E}\rangle_{\Omega}.\end{aligned} \tag{14}$$

The results of this section generalize and extend relations found in Huet [32], Hazanov and Huet [26], Huet [35], Zohdi and Wriggers [60], Zohdi [61] and Zohdi et al. [64] and Zohdi [66].

Remark: For isotropic material responses we have

$$\begin{aligned}
&\langle\kappa^{-1}\rangle_\Omega^{-1} \le \ldots \overset{\hat{\mathrm{L}}}{\kappa^*} \le \overset{\hat{\mathrm{P}}}{\kappa^*} \ \ldots \le \hat{\kappa}^* \le \kappa^* \le \tilde{\kappa}^* \le \ldots \overset{\tilde{\mathrm{M}}}{\kappa^*} \le \overset{\tilde{\mathrm{Z}}}{\kappa^*} \ \ldots \le \langle\kappa\rangle_\Omega \\
&\langle\mu^{-1}\rangle_\Omega^{-1} \le \ldots \overset{\hat{\mathrm{L}}}{\mu^*} \le \overset{\hat{\mathrm{P}}}{\mu^*} \ \ldots \le \hat{\mu}^* \le \mu^* \le \tilde{\mu}^* \le \ldots \overset{\tilde{\mathrm{M}}}{\mu^*} \le \overset{\tilde{\mathrm{Z}}}{\mu^*} \ \ldots \le \langle\mu\rangle_\Omega.
\end{aligned} \tag{15}$$

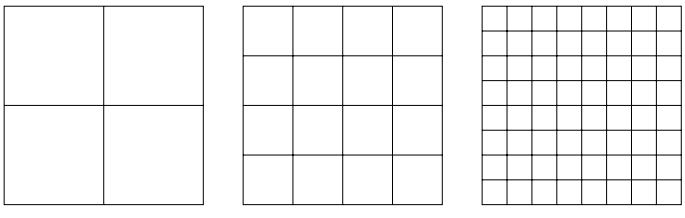

Figure 3. Successively embedded partitions.

4. Moment bounds on population responses

Let us take any effective property, averaged over the *ith* subsample, denoted by Q_i, and correspondingly then A is the average of all of the samples. Let Q^* denote the true effective property. We use the notation $[\tilde{\boldsymbol{I\!E}}^* - \boldsymbol{I\!E}^*] \overset{\mathrm{def}}{=} \mathcal{T} : (\tilde{\boldsymbol{I\!E}}^* - \boldsymbol{I\!E}^*) : \mathcal{T}$, where $\mathcal{T}$ is any arbitrary second order (strain) tensor.

4.1. First order (average) bounds

Equation 14 implies

$$\begin{aligned}
&\boldsymbol{M}_1^{[\overset{\tilde{\mathrm{Z}}}{\boldsymbol{I\!E}}^*{}_i - \overset{\tilde{\mathrm{M}}}{\boldsymbol{I\!E}}^*]} \le \boldsymbol{M}_1^{[\overset{\tilde{\mathrm{Z}}}{\boldsymbol{I\!E}}^*{}_i - \boldsymbol{I\!E}^*]} \le \boldsymbol{M}_1^{[\overset{\tilde{\mathrm{Z}}}{\boldsymbol{I\!E}}^*{}_i - \overset{\hat{\mathrm{P}}}{\boldsymbol{I\!E}}^*]} \le \boldsymbol{M}_1^{[\overset{\tilde{\mathrm{Z}}}{\boldsymbol{I\!E}}^*{}_i - \overset{\hat{\mathrm{L}}}{\boldsymbol{I\!E}}^*]}, \\
&\boldsymbol{M}_1^{[\overset{\hat{\mathrm{L}}}{\boldsymbol{I\!E}}^*{}_i - \overset{\hat{\mathrm{P}}}{\boldsymbol{I\!E}}^*]} \ge \boldsymbol{M}_1^{[\overset{\hat{\mathrm{L}}}{\boldsymbol{I\!E}}^*{}_i - \boldsymbol{I\!E}^*]} \ge \boldsymbol{M}_1^{[\overset{\hat{\mathrm{L}}}{\boldsymbol{I\!E}}^*{}_i - \overset{\tilde{\mathrm{M}}}{\boldsymbol{I\!E}}^*]} \ge \boldsymbol{M}_1^{[\overset{\hat{\mathrm{L}}}{\boldsymbol{I\!E}}^*{}_i - \overset{\tilde{\mathrm{Z}}}{\boldsymbol{I\!E}}^*]}.
\end{aligned} \tag{16}$$

4.2. Second order (standard deviation) bounds

For the second order moments, the shifting theorems imply

$$
\begin{aligned}
\boldsymbol{M}_2^{[\tilde{\boldsymbol{\mathcal{E}}}^*{}_i-\boldsymbol{\mathcal{E}}^*]} &= \boldsymbol{M}_2^{[\tilde{\boldsymbol{\mathcal{E}}}^*{}_i-\tilde{\boldsymbol{\mathcal{E}}}^*]} + \left(\boldsymbol{M}_1^{[\tilde{\boldsymbol{\mathcal{E}}}^*{}_i-\boldsymbol{\mathcal{E}}^*]}\right)^2, \\
\boldsymbol{M}_2^{[\tilde{\boldsymbol{\mathcal{E}}}^*{}_i-\tilde{\boldsymbol{\mathcal{M}}}^*]} &= \boldsymbol{M}_2^{[\tilde{\boldsymbol{\mathcal{E}}}^*{}_i-\tilde{\boldsymbol{\mathcal{E}}}^*]} + \left(\boldsymbol{M}_1^{[\tilde{\boldsymbol{\mathcal{E}}}^*{}_i-\tilde{\boldsymbol{\mathcal{M}}}^*]}\right)^2, \\
\boldsymbol{M}_2^{[\tilde{\boldsymbol{\mathcal{E}}}^*{}_i-\hat{\boldsymbol{\mathcal{L}}}^*]} &= \boldsymbol{M}_2^{[\tilde{\boldsymbol{\mathcal{E}}}^*{}_i-\tilde{\boldsymbol{\mathcal{E}}}^*]} + \left(\boldsymbol{M}_1^{[\tilde{\boldsymbol{\mathcal{E}}}^*{}_i-\hat{\boldsymbol{\mathcal{L}}}^*]}\right)^2, \\
\boldsymbol{M}_2^{[\tilde{\boldsymbol{\mathcal{E}}}^*{}_i-\hat{\boldsymbol{\mathcal{P}}}^*]} &= \boldsymbol{M}_2^{[\tilde{\boldsymbol{\mathcal{E}}}^*{}_i-\tilde{\boldsymbol{\mathcal{E}}}^*]} + \left(\boldsymbol{M}_1^{[\tilde{\boldsymbol{\mathcal{E}}}^*{}_i-\hat{\boldsymbol{\mathcal{P}}}^*]}\right)^2.
\end{aligned}
\tag{17}
$$

and

$$
\begin{aligned}
\boldsymbol{M}_2^{[\hat{\boldsymbol{\mathcal{L}}}^*{}_i-\boldsymbol{\mathcal{E}}^*]} &= \boldsymbol{M}_2^{[\hat{\boldsymbol{\mathcal{L}}}^*{}_i-\hat{\boldsymbol{\mathcal{L}}}^*]} + \left(\boldsymbol{M}_1^{[\hat{\boldsymbol{\mathcal{L}}}^*{}_i-\boldsymbol{\mathcal{E}}^*]}\right)^2, \\
\boldsymbol{M}_2^{[\hat{\boldsymbol{\mathcal{L}}}^*{}_i-\hat{\boldsymbol{\mathcal{P}}}^*]} &= \boldsymbol{M}_2^{[\hat{\boldsymbol{\mathcal{L}}}^*{}_i-\hat{\boldsymbol{\mathcal{L}}}^*]} + \left(\boldsymbol{M}_1^{[\hat{\boldsymbol{\mathcal{L}}}^*{}_i-\hat{\boldsymbol{\mathcal{P}}}^*]}\right)^2, \\
\boldsymbol{M}_2^{[\hat{\boldsymbol{\mathcal{L}}}^*{}_i-\tilde{\boldsymbol{\mathcal{Z}}}^*]} &= \boldsymbol{M}_2^{[\hat{\boldsymbol{\mathcal{L}}}^*{}_i-\hat{\boldsymbol{\mathcal{L}}}^*]} + \left(\boldsymbol{M}_1^{[\hat{\boldsymbol{\mathcal{L}}}^*{}_i-\tilde{\boldsymbol{\mathcal{Z}}}^*]}\right)^2, \\
\boldsymbol{M}_2^{[\hat{\boldsymbol{\mathcal{L}}}^*{}_i-\tilde{\boldsymbol{\mathcal{M}}}^*]} &= \boldsymbol{M}_2^{[\hat{\boldsymbol{\mathcal{L}}}^*{}_i-\hat{\boldsymbol{\mathcal{L}}}^*]} + \left(\boldsymbol{M}_1^{[\hat{\boldsymbol{\mathcal{L}}}^*{}_i-\tilde{\boldsymbol{\mathcal{M}}}^*]}\right)^2.
\end{aligned}
\tag{18}
$$

The results in Equations 16-18 imply

$$
\begin{aligned}
\boldsymbol{M}_2^{[\tilde{\boldsymbol{\mathcal{E}}}^*{}_i-\tilde{\boldsymbol{\mathcal{M}}}^*]} \le \boldsymbol{M}_2^{[\tilde{\boldsymbol{\mathcal{E}}}^*{}_i-\boldsymbol{\mathcal{E}}^*]} \le \boldsymbol{M}_2^{[\tilde{\boldsymbol{\mathcal{E}}}^*{}_i-\hat{\boldsymbol{\mathcal{P}}}^*]} \le \boldsymbol{M}_2^{[\tilde{\boldsymbol{\mathcal{E}}}^*{}_i-\hat{\boldsymbol{\mathcal{L}}}^*]} \\
\boldsymbol{M}_2^{[\hat{\boldsymbol{\mathcal{L}}}^*{}_i-\hat{\boldsymbol{\mathcal{P}}}^*]} \le \boldsymbol{M}_2^{[\hat{\boldsymbol{\mathcal{L}}}^*{}_i-\boldsymbol{\mathcal{E}}^*]} \le \boldsymbol{M}_2^{[\hat{\boldsymbol{\mathcal{L}}}^*{}_i-\tilde{\boldsymbol{\mathcal{M}}}^*]} \le \boldsymbol{M}_2^{[\hat{\boldsymbol{\mathcal{L}}}^*{}_i-\tilde{\boldsymbol{\mathcal{Z}}}^*]}
\end{aligned}
\tag{19}
$$

Remark: In the case of isotropy, the moment results hold for the effective shear

and bulk moduli individually.

4.3. Third order (skewness) bounds

From Equation 5, we may write the skewnesses as

$$
\begin{aligned}
M_3^{[\tilde{\boldsymbol{IE}}^*{}_i - \boldsymbol{IE}^*]} &= M_3^{[\tilde{\boldsymbol{IE}}^*{}_i - \tilde{\boldsymbol{IE}}^*]} + M_1^{[\tilde{\boldsymbol{IE}}^*{}_i - \boldsymbol{IE}^*]} M_2^{[\tilde{\boldsymbol{IE}}^*{}_i - \boldsymbol{IE}^*]} \\
&\quad + 2M_1^{[\tilde{\boldsymbol{IE}}^*{}_i - \boldsymbol{IE}^*]} M_2^{[\tilde{\boldsymbol{IE}}^*{}_i - \tilde{\boldsymbol{IE}}^*]}, \\
M_3^{[\tilde{\boldsymbol{IE}}^*{}_i - \tilde{\boldsymbol{IM}}^*]} &= M_3^{[\tilde{\boldsymbol{IE}}^*{}_i - \tilde{\boldsymbol{IE}}^*]} + M_1^{[\tilde{\boldsymbol{IE}}^*{}_i - \tilde{\boldsymbol{IM}}^*]} M_2^{[\tilde{\boldsymbol{IE}}^*{}_i - \tilde{\boldsymbol{IM}}^*]} \\
&\quad + 2M_1^{[\tilde{\boldsymbol{IE}}^*{}_i - \tilde{\boldsymbol{IM}}^*]} M_2^{[\tilde{\boldsymbol{IE}}^*{}_i - \tilde{\boldsymbol{IE}}^*]}, \\
M_3^{[\tilde{\boldsymbol{IE}}^*{}_i - \hat{\boldsymbol{IL}}^*]} &= M_3^{[\tilde{\boldsymbol{IE}}^*{}_i - \tilde{\boldsymbol{IE}}^*]} + M_1^{[\tilde{\boldsymbol{IE}}^*{}_i - \hat{\boldsymbol{IL}}^*]} M_2^{[\tilde{\boldsymbol{IE}}^*{}_i - \hat{\boldsymbol{IL}}^*]} \\
&\quad + 2M_1^{[\tilde{\boldsymbol{IE}}^*{}_i - \hat{\boldsymbol{IL}}^*]} M_2^{[\tilde{\boldsymbol{IE}}^*{}_i - \tilde{\boldsymbol{IE}}^*]}, \\
M_3^{[\tilde{\boldsymbol{IE}}^*{}_i - \hat{\boldsymbol{IP}}^*]} &= M_3^{[\tilde{\boldsymbol{IE}}^*{}_i - \tilde{\boldsymbol{IE}}^*]} + M_1^{[\tilde{\boldsymbol{IE}}^*{}_i - \hat{\boldsymbol{IP}}^*]} M_2^{[\tilde{\boldsymbol{IE}}^*{}_i - \hat{\boldsymbol{IP}}^*]} \\
&\quad + 2M_1^{[\tilde{\boldsymbol{IE}}^*{}_i - \hat{\boldsymbol{IP}}^*]} M_2^{[\tilde{\boldsymbol{IE}}^*{}_i - \tilde{\boldsymbol{IE}}^*]},
\end{aligned}
\tag{20}
$$

and as

$$
\begin{aligned}
M_3^{[\hat{\boldsymbol{IL}}^*{}_i - \boldsymbol{IE}^*]} &= M_3^{[\hat{\boldsymbol{IL}}^*{}_i - \hat{\boldsymbol{IL}}^*]} + M_1^{[\hat{\boldsymbol{IL}}^*{}_i - \boldsymbol{IE}^*]} M_2^{[\hat{\boldsymbol{IL}}^*{}_i - \boldsymbol{IE}^*]} \\
&\quad + 2M_1^{[\hat{\boldsymbol{IL}}^*{}_i - \boldsymbol{IE}^*]} M_2^{[\hat{\boldsymbol{IL}}^*{}_i - \hat{\boldsymbol{IL}}^*]}, \\
M_3^{[\hat{\boldsymbol{IL}}^*{}_i - \hat{\boldsymbol{IP}}^*]} &= M_3^{[\hat{\boldsymbol{IL}}^*{}_i - \hat{\boldsymbol{IL}}^*]} + M_1^{[\hat{\boldsymbol{IL}}^*{}_i - \hat{\boldsymbol{IP}}^*]} M_2^{[\hat{\boldsymbol{IL}}^*{}_i - \hat{\boldsymbol{IP}}^*]} \\
&\quad + 2M_1^{[\hat{\boldsymbol{IL}}^*{}_i - \hat{\boldsymbol{IP}}^*]} M_2^{[\hat{\boldsymbol{IL}}^*{}_i - \hat{\boldsymbol{IL}}^*]}, \\
M_3^{[\hat{\boldsymbol{IL}}^*{}_i - \tilde{\boldsymbol{IZ}}^*]} &= M_3^{[\hat{\boldsymbol{IL}}^*{}_i - \hat{\boldsymbol{IL}}^*]} + M_1^{[\hat{\boldsymbol{IL}}^*{}_i - \tilde{\boldsymbol{IZ}}^*]} M_2^{[\hat{\boldsymbol{IL}}^*{}_i - \tilde{\boldsymbol{IZ}}^*]} \\
&\quad + 2M_1^{[\hat{\boldsymbol{IL}}^*{}_i - \tilde{\boldsymbol{IZ}}^*]} M_2^{[\hat{\boldsymbol{IL}}^*{}_i - \hat{\boldsymbol{IL}}^*]}, \\
M_3^{[\hat{\boldsymbol{IL}}^*{}_i - \tilde{\boldsymbol{IM}}^*]} &= M_3^{[\hat{\boldsymbol{IL}}^*{}_i - \hat{\boldsymbol{IL}}^*]} + M_1^{[\hat{\boldsymbol{IL}}^*{}_i - \tilde{\boldsymbol{IM}}^*]} M_2^{[\hat{\boldsymbol{IL}}^*{}_i - \tilde{\boldsymbol{IM}}^*]}
\end{aligned}
\tag{21}
$$

$$+ 2\boldsymbol{M}_1^{[\hat{\boldsymbol{I\!E}}^*{}_i - \tilde{\boldsymbol{I\!E}}^*]}\boldsymbol{M}_2^{[\hat{\boldsymbol{I\!E}}^*{}_i - \hat{\boldsymbol{I\!E}}^*]},$$

The previous expressions imply

$$\begin{aligned}
&\boldsymbol{M}_3^{[\bar{\boldsymbol{I\!E}}^*{}_i - \tilde{\boldsymbol{I\!E}}^*]} \leq \boldsymbol{M}_3^{[\bar{\boldsymbol{I\!E}}^*{}_i - \boldsymbol{I\!E}^*]} \leq \boldsymbol{M}_3^{[\bar{\boldsymbol{I\!E}}^*{}_i - \hat{\boldsymbol{I\!E}}^*]} \leq \boldsymbol{M}_3^{[\bar{\boldsymbol{I\!E}}^*{}_i - \hat{\boldsymbol{I\!E}}^*]} \\
&\boldsymbol{M}_3^{[\hat{\boldsymbol{I\!E}}^*{}_i - \hat{\boldsymbol{I\!E}}^*]} \geq \boldsymbol{M}_3^{[\hat{\boldsymbol{I\!E}}^*{}_i - \boldsymbol{I\!E}^*]} \geq \boldsymbol{M}_3^{[\hat{\boldsymbol{I\!E}}^*{}_i - \tilde{\boldsymbol{I\!E}}^*]} \geq \boldsymbol{M}_3^{[\hat{\boldsymbol{I\!E}}^*{}_i - \bar{\boldsymbol{I\!E}}^*]}.
\end{aligned} \tag{22}$$

The derived results allow one to bound, above and below, the unknown SRVE response in terms of the ensembles averages. Using similar techniques, bounds on even higher order moments, such as the kurtosis (fourth moment), which measures the peakedness of the distribution, are possible.

References

[1] Aboudi, J., *Mechanics of Composite Materials-a Unified Micromechanical Approach*. Elsevier, 29. 1992.

[2] M. Ainsworth and J. T. Oden, *A Posterori Error Estimation in Finite Element Analysis*. John-Wiley 2000.

[3] M. Amieur, S. Hazanov and C. Huet, Numerical and experimental study of size and boundary conditions effects on the apparent properties of specimens not having the representative volume. In *Micromechanics of Concrete and Cementitious Composite*, (ed. C. Huet) 1993.

[4] B. Budiansky, On the elastic moduli of some heterogeneous materials. *Journal of the Mechanics and Physics of Solids.* **13** (1965), 223–227.

[5] W. Chen and J. Fish, A dispersive model for wave propagation in periodic heterogeneous media based on homogenization with multiple spatial and temporal scales. *Journal of Applied Mechanics* **68** (2001), 153–161.

[6] J. Fish and A. Wagiman, Multiscale finite element method for a locally nonperiodic heterogeneous medium. *Comput. Mech.* **12** (1993), 164–180.

[7] J. Fish, M. Pandheeradi and V. Belsky, An efficient multilevel solution scheme for large scale nonlinear systems. *International Journal for Numerical Methods in Engineering* **38** (1995), 1597–1610.

[8] J. Fish and V. Belsky, Multigrid method for periodic heterogeneous media Part I: Convergence studies for one dimensional case, *Computer Methods in Applied Mechanics and Engineering* **126** (1995) 1–16.

[9] J. Fish and V. Belsky, Multigrid method for periodic heterogeneous media Part II: Multiscale modeling and quality control in multidimensional case, *Computer Methods in Applied Mechanics and Engineering.* **126** (1995), 17–38.

[10] J. Fish and V. Belsky, Generalized aggregation multilevel solver. *International Journal for Numerical Methods in Engineering.* **40** (1997), 4341–4361.

[11] J. Fish, K. Shek, M. Pandheeradi and M. S. Shephard, Computational plasticity for composite structures based on mathematical homogenization: Theory and practice *Computer Methods in Applied Mechanics and Engineering.* **148** (1997), 53–73.

[12] J. Fish, Q. Yu and K. L. Shek, Computational damage mechanics for composite materials based on mathematical homogenization. *International Journal for Numerical Methods in Engineering.* **45** (1999), 1657–1679.

[13] J. Fish and K. Shek, Finite deformation plasticity for composite structures: Computational models and adaptive strategies *Computer Methods in Applied Mechanics and Engineering* **172** (1999), 145–174.

[14] J. Fish and A. Ghouli, Multiscale analytical sensitivity analysis for composite materials. *International Journal for Numerical Methods in Engineering.* **50** (2001), 1501–1520.

[15] J. Fish and Q. Yu, Multiscale damage modeling for composite materials: theory and computational framework. *International Journal for Numerical Methods in Engineering.* **52** (2001), 161–192.

[16] J.Fish and W. Chen, Uniformly valid multiple spatial-temporal scale modeling for wave propagation in heterogeneous media. *Mechanics of Composite Materials and Structures* **8** (2001), 81–99.

[17] Y. Fu, K. Klimkowski, G. J. Rodin, E. Berger, J. C. Browne, J. K. Singer, R. A. Van de Geijn and K. Vemaganti, Fast solution method for three-dimensional many-particle problems of linear elasticity. *The International Journal of Numerical Methods in Engineering* **42** (1998), 1215–1229.

[18] S. Ghosh and S. N. Mukhopadhyay, A material based finite element analysis of heterogeneous media involving Dirichlet tessellations, *Computer Methods in Applied Mechanics and Engineering* **104** (1993, 211–247.

[19] S. Ghosh and S. Moorthy, Elastic-plastic analysis of arbitrary heterogeneous materials with the Voronoi cell finite element method. *Computer Methods in Applied Mechanics and Engineering* **121** (1995), 373–409.

[20] S. Ghosh, L. Kyunghoon and S. Moorthy, Two scale analysis of heterogeneous elastic-plastic materials with asymptotic homogenization and Voronoi cell finite element model. *Computer Methods in Applied Mechanics and Engineering* **132** (1996), 63–116.

[21] S. Ghosh and S. Moorthy, Particle fracture simulation in non-uniform microstructures of metal-matrix composites. *Acta mater.* **46** (1998), 965–982.

[22] S. Ghosh, K. Lee and P. Raghavan, A multi-level computational model for multi-scale damage analysis in composite and porous materials. *International Journal of Solids and Structures* **38** (2001), 2335–2385.

[23] S. Ghosh, Y. Ling, B. Majumdar and R. Kim, Interfacial debonding analysis in multiple fiber reinforced composites. *Mechanics of Materials* **32** (2001), 562–591.

[24] A. Guidoum and P. Navi, Numerical simulation of thermo-mechanical behaviour of concrete through a 3-D granular cohesive model. In C. Huet (Ed.) *Micromechanics of Concrete and Cementitious Composites*, Presses Polytechniques et Universitaires Romandes, Lausanne 1993, pp. 213–228.

[25] A. Guidoum, Simulation numérique 3D des comportements des bétons en tant que composites granulaires. Doctoral Dissertation No 1310. Ecole Polytechnique de Lausanne, Switzerland 1994

[26] S. Hazanov and C. Huet, Order relationships for boundary conditions effect in heterogeneous bodies smaller than the representative volume. *Journal of the Mechanics and Physics of Solids.* **42** (1994), 1995–2011.

[27] S. Hazanov and M. Amieur, On overall properties of elastic heterogeneous bodies smaller than the representative volume. *Int. J. Eng. Science* **33** (1995), 1289–1301.

[28] R. Hill, The elastic behaviour of a crystalline aggregate. *Proc. Phys. Soc. (Lond.)* **A65**, (1952), 349–354.

[29] C. Huet, Remarques sur l'assimilation d'un matériau hétérogéne à un milieu continu équivalent. In C. Huet and A. Zaoui (eds.), *Rheological Behaviour and Structure of Materials.* Presses ENPC, Paris 1981. pp. 231–245.

[30] C. Huet, Universal conditions for assimilation of a heterogeneous material to an effective medium. *Mechanics Research Communications* **9** (1982), 165–170.

[31] C. Huet, On the definition and experimental determination of effective constitutive equations for heterogeneous materials. *Mechanics Research Communications.* **11** (1984), 195–200.

[32] C. Huet, Application of variational concepts to size effects in elastic heterogeneous bodies. *Journal of the Mechanics and Physics of Solids* **38** (1990), 813–841.
[33] C. Huet, Hierarchies and bounds for size effects in heterogeneous bodies. In *Continuum Models and Discrete Systems*, G. A. Maugin (ed.) Vol. **2**, 1991, pp. 127–134.
[34] C. Huet, An integrated micromechanics and statistical continuum thermodynamics approach for studying the fracture behaviour of microcracked heterogeneous materials with delayed response. *Engineering Fracture Mechanics, Special Issue* **58** (1997), 459–556.
[35] C. Huet, Coupled size and boundary condition effects in viscoelastic heterogeneous bodies. *Mechanics of Materials.* **31** (1999), 787–829.
[36] V. V. Jikov, S. M. Kozlov and O. A. Olenik, *Homogenization of Differential Operators and Integral Functionals*. Springer-Verlag, 1994.
[38] K. Lee, S. Moorthy and S. Ghosh, Multiple scale computational model for damage in composite materials, Effective properties of composite materials with periodic microstructure: a computational approach *Computer Methods in Applied Mechanics and Engineering* **172** (1994) 175–201.
[39] P. Le Tallec, Domain decomposition methods in computational mechanics. *Computational Mechanics Advances.* **1** (1994), 121–220.
[40] M. Li, S. Ghosh and O. Richmond, An experimental-computational approach to the investigation of damage evolution in discontinuously reinforced aluminum matrix composite. *Acta mater.* **47** (1999), 3515–3532.
[41] J. C. Michel, H. Moulinec and P. Suquet, Effective properties of composite materials with periodic microstructure: a computational approach *Computer Methods in Applied Mechanics and Engineering* **172** (1999), 109–143.
[42] N. Moes, J. T. Oden and T. I. Zohdi, Investigation of the interaction of numerical error and modeling error in the Homogenized Dirichlet Projection Method. *Computer Methods in Applied Mechanics and Engineering.* **159** (1998), 79–101.
[43] S. Moorthy and S. Ghosh, Adaptivity and convergence in the Voronoi cell finite element model for analyzing heterogeneous materials. *Computer Methods in Applied Mechanics and Engineering* **185** (2000), 37–74.
[44] H. Moulinec and P. Suquet, A numerical method for computing the overall response of nonlinear composites with complex microstructure. *Computer Methods in Applied Mechanics and Engineering* **157** (1998), 69–94.
[45] T. Mura, *Micromechanics of Defects in Solids*, 2nd edition, Kluwer Academic Publishers 1993.
[46] S. Nemat-Nasser and M. Hori, *Micromechanics: Overall Properties of Heterogeneous Solids.* 2nd edition. Elsevier, Amsterdam 1999.
[47] J. T. Oden T. I. and Zohdi, Analysis and adaptive modeling of highly heterogeneous elastic structures. *Computer Methods in Applied Mechanics and Engineering.* **148** (1997), 367–391.
[48] J. T. Oden and K. Vemaganti, Adaptive hierarchical modeling of heterogeneous structures. *Physica D*, **133** (1999), 404–415.
[49] J. T. Oden, K. Vemaganti and N. Moes, Hierarchical modeling of heterogeneous solids. *Computer Methods in Applied Mechanics and Engineering* **172** (1997), 1–27.
[50] P. Raghavan, S. Moorthy, S. Ghosh and N. J. Pagano, Revisiting the composite laminate problem with an adaptive multi-level computational model. *Composites Science and Technology* **61** (2001), 1017–1040.
[51] A. Reuss, Berechnung der Fliessgrenze von Mischkristallen auf Grund der Plastizitätsbedingung für Einkristalle. *Z. angew. Math. Mech.* **9** (1929), 49–58.
[52] S. Torquato, Random heterogeneous media: microstructure and improved bounds on effective properties. *Appl. Mech. Rev.* **44** (1991), 37–76.
[53] S. Torquato, Effective stiffness tensor of composite media I. Exact series expansions. *Journal of the Mechanics and Physics of Solids.* **45** (1997), 1421–1448.
[54] S. Torquato, Effective stiffness tensor of composite media II. Applications to isotropic dispersions. *Journal of the Mechanics and Physics of Solids* **46** (1998), 1411–1440.

[55] S. Torquato, *Random Heterogeneous Materials: Microstructure and Macroscopic Properties*, Springer-Verlag, New York 2001.
[56] K. S. Vemaganti and J. T. Oden, Estimation of local modeling error and goal-oriented adaptive modeling of heterogeneous materials. *Computer Methods in Applied Mechanics and Engineering* **190** (2001), 6089–6124.
[57] W. Voigt, Über die Beziehung zwischen den beiden Elastizitätskonstanten isotroper Körper. *Wied. Ann.* **38** (1889), 573–587.
[58] R. Wentorf, R. Collar, M. S. Shephard and J. Fish, Automated modeling for complex woven mesostructures. *Comp. Meth. Appl. Mech. Engng.* **172** (1999), 273–291.
[59] T. I. Zohdi, J. T. Oden and G. J. Rodin, Hierarchical modeling of heterogeneous bodies. *Computer Methods in Applied Mechanics and Engineering.* **138** (1996), 273–298.
[60] T. I. Zohdi and P. Wriggers, A domain decomposition method for bodies with microstructure based upon material regularization. *The International Journal of Solids and Structures.* **36** (1999), 2507–2526.
[61] T. I. Zohdi, Overall solution-difference bounds on the effects of material inhomogeneities. *The Journal of Elasticity.* **58** (2000), 249–255.
[62] T. I. Zohdi and P. Wriggers, Aspects of the computational testing of the mechanical properties of microheterogeneous material samples. *The International Journal of Numerical Methods in Engineering.* **50** (2001), 2573–2599.
[63] T. I. Zohdi and P. Wriggers, Computational micro-macro material testing. *Archives of Computational Methods in Engineering.* **8** (2001), 131–228.
[64] T. I. Zohdi, P. Wriggers and C. Huet, A method of substructuring large-scale computational micromechanical problems. *Computer Methods in Applied Mechanics and Engineering* **190** (2001), 5639–5656.
[65] T. I. Zohdi, Computational optimization of vortex manufacturing of advanced materials. *Computer Methods in Applied Mechanics and Engineering* **190** (2001), 6231–6256.
[66] T. I. Zohdi, Bounding envelopes in multiphase material design. *The Journal of Elasticity* **66** (2002), 47-62.

T. I. Zohdi
Department of Mechanical Engineering
6195 Etcheverry Hall
University of California
Berkeley, CA, 94720-1740
USA
e-mail: zohdi@newton.berkeley.edu

(Received: December 11, 2001)